Clim. Past Discuss., 8, 6051–6091, 2012
www.clim-past-discuss.net/8/6051/2012/
doi:10.5194/cpd-8-6051-2012

Climate of the Past Discussions

Glacial-interglacial dynamics of Antarctic firn columns: comparison between simulations and ice core air-δ^{15}N measurements

E. Capron[1,2], A. Landais[2], D. Buiron[3], A. Cauquoin[2], J. Chappellaz[3], M. Debret[3,4], J. Jouzel[2], M. Leuenberger[5], P. Martinerie[3], V. Masson-Delmotte[2], R. Mulvaney[1], F. Parrenin[3], and F. Prié[2]

[1]British Antarctic Survey, NERC, High Cross, Madingley Road, Cambridge CB3 0ET, UK
[2]Institut Pierre-Simon Laplace/Laboratoire des Sciences du Climat et de l'Environnement, UMR8212, CEA-CNRS-UVSQ, 91191 Gif-sur-Yvette, France
[3]UJF – Grenoble 1/CNRS, Laboratoire de Glaciologie et Géophysique de l'Environnement (LGGE), UMR5183, CNRS, 38041 Grenoble, France
[4]Laboratoire Morphodynamique Continentale et Côtière (M2C), UMR6143, Université de Caen Basse-Normandie et Université de Rouen, 14000 Caen/76821 Mont-Saint-Aignan, France
[5]Climate and Environmental Physics, Physics Institute, and Oeschger Centre for Climate Change Research, University of Bern, Sidlerstrasse 5, 3012 Bern, Switzerland

Received: 8 November 2012 – Accepted: 28 November 2012 – Published: 4 December 2012

Correspondence to: E. Capron (ecap@bas.ac.uk)

Published by Copernicus Publications on behalf of the European Geosciences Union.

CPD
8, 6051–6091, 2012

Abstract

Correct estimate of the firn lock-in depth is essential for correctly linking gas and ice chronologies in ice cores studies. Here, two approaches to constrain the firn depth evolution in Antarctica are presented over the last deglaciation: output of a firn densification model and measurements of $\delta^{15}N$ of N_2 in air trapped in ice core. Since the firn densification process is largely governed by surface temperature and accumulation rate, we have investigated four ice cores drilled in coastal (Berkner Island, BI, and James Ross Island, JRI) and semi coastal (TALDICE and EPICA Dronning Maud Land, EDML) Antarctic regions. Combined with available $\delta^{15}N$ measurements performed from the EPICA Dome C (EDC) site, the studied regions encompass a large range of surface accumulation rate and temperature conditions.

While firn densification simulations are able to correctly represent most of the $\delta^{15}N$ trends over the last deglaciation measured in the EDC, BI, TALDICE and EDML ice cores, they systematically fail to capture BI and EDML $\delta^{15}N$ glacial levels, a mismatch previously seen for Central East Antarctic ice cores. Using empirical constraints of the EDML gas-ice depth offset during the Laschamp event ($\sim$ 41 ka), we can rule out the existence of a large convective zone as the explanation of the glacial firn model- $\delta^{15}N$ data mismatch for this site. The good match between modelled and measured $\delta^{15}N$ at TALDICE as well as the lack of any clear correlation between insoluble dust concentration in snow and $\delta^{15}N$ records in the different ice cores suggest that past changes in loads of impurities are not the only main driver of glacial-interglacial changes in firn lock-in depth.

We conclude that firn densification dynamics may instead be driven mostly by accumulation rate changes. The mismatch between modelled and measured $\delta^{15}N$ may be due to inaccurate reconstruction of past accumulation rate or underestimated influence of accumulation rate in firnification models.

CPD
8, 6051–6091, 2012

1 Introduction

Antarctic ice cores have provided outstanding records of past changes in climate and atmospheric composition (e.g. Jouzel et al., 2007; Loulergue et al., 2008; Lüthi et al., 2008; Schilt et al., 2010). A precise evaluation of the phase relationship between changes in local surface temperature and atmospheric composition remains however challenged by the fact that air is trapped only at the bottom of the firn, i.e. a 60–120 m permeable layer below the surface where snow progressively densifies into ice. This leads to trapped air at the bubble Close Off-Depth (COD) that is surrounded by ice as old as several hundred to up to ∼ 5500 yr in the case of Central Antarctic sites, such as for the European Project for Ice Coring in Antarctica Dome C (EDC) site (Loulergue et al., 2007; Fig. 1). The gas/ice offset can be characterized by (i) the ice age-gas age difference at a given depth, noted Δage or alternatively by (ii) the depth difference between gas and ice of a given age, noted Δdepth. Constraining the firn structure is crucial to accurately estimate Δage and Δdepth and reduce uncertainties in ice and gas chronologies, in particular for clarifying the exact timing between CO_2 concentration and Antarctic surface temperature during deglaciations (Caillon et al., 2001; Fischer, 1999; Monnin et al., 2001; Pedro et al., 2011; Shakun et al., 2012; Parrenin et al., 2012a).

Firn densification models have been specifically developed to build ice core gas chronologies, which requires estimating Δage or Δdepth (e.g. Bender et al., 2006; Blunier et al., 2004; Loulergue et al., 2007). They assume a continuous snow material where densification, and thus the COD, is mainly dependent on accumulation rate, surface temperature and surface density (Arnaud et al., 2000; Goujon et al., 2003; Herron and Langway, 1980; Pimienta, 1987; Schwander et al., 1993).

The isotopic composition of nitrogen (δ^{15}N of N_2, hereafter δ^{15}N) in air trapped in ice core also provide information on past firn depth. Indeed, in the absence of any rapid temperature change, δ^{15}N variations are only caused by gravitational fractionation, which leads to an enrichment of the trapped air in heavy isotopes proportionally to the

CPD
8, 6051–6091, 2012

Diffusive Colum Height (DCH). It follows the barometric equation (Eq. 1):

$$\delta_{grav} = \left[\exp\left(\frac{\Delta m g z}{RT}\right) - 1\right] \times 1000 \quad (1)$$

where Δm is the mass difference (g mol^{-1}; for the case of δ^{15}N, it is the mass difference between ^{15}N and ^{14}N), g is the gravitation acceleration (m s^{-2}), z, the Diffusive Column Height (m), R, the gas constant (J K^{-1} mol^{-1}) and T, the firn temperature (K).

The convective zone, in the upper part of the firn, is characterized by convective mixing that overwhelms molecular diffusion and prevents isotopic fractionation. Assuming that this convective zone is negligible, the DCH provides an estimate of the Lock-In Depth (LID), which represents the depth where the gas diffusion becomes negligible. Sites where firn air studies have been conducted so far are characterized by a convective zone spanning from 0 m to up to 20 m depth (Landais et al., 2006; Kawamura et al., 2006; Severinghaus et al., 2010). The LID is generally slightly smaller than the COD due to the presence at the bottom of the firn of a non-diffusive zone, where the micropores are not entirely closed but the air is not moving vertically any longer. Based on a model-data comparison, Landais et al. (2006) report a non-diffusive zone usually of only few meters for current Antarctic sites but which could potentially reach 13 m.

The most recent firn densification models have been evaluated against modern firn air δ^{15}N observations spanning a range of mean annual temperatures at various Antarctic and Greenlandic sites (from −19 °C to −55.5 °C for surface temperature and from 152 to 2.4 cm ice equivalent per year (hereafter noted ice eq. yr^{-1}) for the accumulation rate; Goujon et al., 2003; Landais et al., 2006). These models are also able to reproduce the glacial LID inferred from δ^{15}N records from various Greenland ice cores (e.g. Huber et al., 2006; Landais et al., 2004; NorthGRIP community members, 2004), and from the Antarctic Byrd ice core (Sowers et al., 1992). Glacial climatic conditions at these sites are within the present range of surface parameters for which the models have been evaluated, e.g. LGM mean surface temperature of about −43 °C and −52 °C

CPD
8, 6051–6091, 2012

and LGM mean accumulation rate of ∼ 5 and ∼ 6 cm ice eq. yr^{-1} for Byrd (Blunier et al., 1998) and NorthGRIP respectively (Johnsen et al., 2001).

In several Antarctic sites characterized by low accumulation rates (Vostok, EDC, Dome F), firn models suggest an increased LID during glacial time, opposite to the LID evolution inferred from $\delta^{15}N$ measurements. While a decrease in accumulation leads to simulate a shallower LID, decreased temperatures have an opposite effect which dominates the overall result (Fig. 2). This model-data mismatch has been largely discussed by Caillon et al. (2001), Landais et al. (2006) and Dreyfus et al. (2010).

First, as firn models use semi-empirical relationships between surface density, temperature, and accumulation rate, Bender et al. (2006) suggested that outside the range of observations under present-day climate, the extrapolation of these empirical relationships may be incorrect. Alternatively, Landais et al. (2006) proposed that the relationships between water stable isotopes, temperature and accumulation used to produce climatic scenarios to force firn models may be incorrect (Landais et al., 2006). These two potential explanations for the model-data $\delta^{15}N$ mismatch rely on the common assumption that the physics of firnification models is globally correct, and that firn model outputs can be reconciled with $\delta^{15}N$ data after adjustments of the forcing scenarios and/or of the modelled influences of accumulation rate and temperature on the firn LID, especially for inland sites characterized by low temperatures and accumulation rates (here called Hypothesis A).

Alternatively, Caillon et al. (2001) and Dreyfus et al. (2010) suggest that the discrepancy between measured $\delta^{15}N$ and modelled $\delta^{15}N$ is not due to errors in firn model or climate forcing scenario, but rather to the presence of a deep convective zone under glacial conditions (here called Hypothesis B) linked to an increased firn permeability in periods of low accumulation rate (Courville et al., 2007). While this process is not implemented in firn models (which do not represent permeability), firnification models should however still correctly predict the LID, and thus Δage and Δdepth. Indeed, only $\delta^{15}N$ should be affected since the DCH would be reduced by the depth of the convective zone with respect to the LID.

CPD
8, 6051–6091, 2012

Recently, Hörshold et al. (2012) have demonstrated that the snow/ice impurity content may have a significant impact on the densification process (hereafter referred as Hypothesis C), with a decrease in firn depth at increasing impurity levels. At the moment, no parameterization of this effect is available for implementation in firn models. If this hypothesis is correct, then our model-data mismatch should coincide with changes in ice core records of impurity content (e.g. insoluble dust or Ca^{2+} concentrations).

Due to the mismatch between firn densification models and $\delta^{15}N$ data, different results have been obtained using one or other approach for constraining ice core gas chronologies (e.g. Buiron et al., 2011; Loulergue et al., 2007; Bazin et al., 2012). Blunier et al. (2004) and Bender et al. (2006) have judged the LID reconstruction method based on $\delta^{15}N$ unsatisfactory. However, for EDC, a recent study has compared a variety of methods for estimating Δdepth and concluded that the LID calculated from $\delta^{15}N$ without any convective zone is appropriate for estimating past Δdepth variations (Parrenin et al., 2012b).

Here, we present published and new measurements of $\delta^{15}N$ and simulations of firn densification over the last deglaciation for five Antarctic sites: Dome C (EPICA Dome C ice core, EDC), Kohnen Station (EPICA Dronning Maud Land ice core, EDML), Talos Dome (TALDICE ice core), Berkner Island (BI ice core) and James Ross Island (JRI ice core). These sites offer surface climatic conditions spanning a very large range of accumulation rates and temperatures. Each of these sites provides also a specific case due to inter-site differences in latitude (and therefore insolation), elevation and distance to the nearest open ocean (Fig. 1). During glacial periods, the coastal or semi-coastal sites are expected to undergo surface temperature and accumulation rate that fall within the densification model empirical validity range. Each of those sites is also characterised by a specific magnitude of glacial-interglacial changes in local insoluble dust concentration (Albani et al., 2012; Lambert et al., 2012; Ruth et al., 2008), allowing us to test Hypothesis C. Using these new datasets, together with water isotope profiles and tests conducted with firn models, we investigate and discuss the

CPD
8, 6051–6091, 2012

different hypotheses presented above and their ability to explain the past firn structure dynamics for semi-coastal and coastal Antarctic sites.

In the following, the analytical method for δ^{15}N measurements is summarized (Sect. 2). Simulations of firn densification during the last glacial-interglacial transition are conducted for the five ice core sites, and discussed (Sect. 3). The new JRI, BI and TALDICE δ^{15}N profiles are described and compared with existing profiles from the EPICA ice cores (EDML and EDC) and firn modelling results (Sect. 4). The mechanisms governing past firn structure evolution in Antarctica are finally discussed (Sect. 5).

2 Measuring δ^{15}N from trapped air in ice: analytical procedure

Here, we complement existing ice core δ^{15}N data from EDC and EDML sites (Dreyfus et al., 2010; Landais et al., 2006) by additional measurements on the EDML ice core and new data measured on the BI, TALDICE and JRI ice cores recently drilled (Fig. 1).

New air isotopic measurements were performed at the Laboratoire des Sciences du Climat et de l'Environnement between 2007 and 2011, during several measurement periods, using a melt-refreeze technique (Landais et al., 2003; Sowers et al., 1989) to extract fossil air from the ice (Table 1). Air samples were then analysed on a 10-collector Delta V Plus (ThermoElectron Corporation) isotope ratio mass spectrometer which allows simultaneous measurements of $m/z = 28$, 29, 30, 32, 33, 34, 36, 38, 40 and 44. Corrections for pressure imbalance and chemical interferences of CO_2 and $\delta O_2/N_2$ were applied to improve the measurement precision following the procedure fully described in Severinghaus et al. (2001) and Landais et al. (2003). The analytical precision over a given measurement period is calculated as the pooled standard deviation of depth pairs (Severinghaus et al., 2001) and is presented in Table 1. The pooled standard deviation for each dataset varies from 0.005 ‰ for the JRI dataset to up to 0.022 ‰ for the EDML dataset. It does not affect the following discussion because the amplitude of the δ^{15}N variations considered here is much larger.

CPD
8, 6051–6091, 2012

In order to constrain the JRI age scale, we used the measurements of $\delta^{18}O$ of O_2 associated with a pooled standard deviation of 0.032 ‰ (see Table 1).

3 Modelling past $\delta^{15}N$ variations: method

3.1 Firn densification models

The sophisticated firnification model of Goujon et al. (2003), hereafter referred as the Goujon model, has been applied to EDML, TALDICE and BI sites. It is an improved version of the dynamic model of Arnaud et al. (2000), hereafter referred as the Arnaud model, which relies on physical processes of pressure sintering to describe the relationships between density, surface temperature and accumulation rate, while some parameters have been fitted also onto density profiles. By taking into account heat diffusion in firn and ice sheet, the Goujon model allows to predict the LID with higher confidence than in static firn models.

However, for the JRI ice core, the lack of a robust and continuous chronology over the last deglaciation and the glacial period prevent us from applying the Goujon model. At this site, we use a static version of the Arnaud model to simulate $\delta^{15}N$ mean level for LGM (Last Glacial Maximum) climatic conditions and one $\delta^{15}N$ mean level for EH (Early Holocene) climatic conditions.

The Goujon model requires a depth-age correspondence for thermal diffusion calculations. Simulating the LID requires us to define a closed porosity threshold. Loulergue et al. (2007) estimate a LID taken at 5 % of closed porosity while Parrenin et al. (2012b) used a 20 % of closed porosity for LID calculations. Based on firn air measurements, Goujon et al. (2003) suggest that the firn gas diffusion stops at closed porosity ranging from 21 % to 13 %. In this study, we set the models to define the past changes in LID taken at 21 % of closed porosity. Then, we deduced $\delta^{15}N$ from Eq. (1). Note that the choice of the threshold on the closed porosity has no impact on the modelled LID evolution over the deglaciation discussed in this paper.

CPD
8, 6051–6091, 2012

3.2 Ice core timescales

Table 2 provides information on the gas and ice timescales onto which our new results have been transferred. Large uncertainties on the ice flow arise from the particular configuration of the Berkner Island drilling site, which may have been affected by the expansion of the East Antarctic ice sheet during the glacial period (Mulvaney et al., 2012). Therefore, the inverse dating method first developed for the Vostok ice core (Parrenin et al., 2004) has not been applied to build a gas and ice chronology at this site. The gas age scale was established by matching BI gas records (CH_4 and CO_2) with gas records from EPICA Dome C (EDC), Byrd and Vostok on the EDC3 chronology (Parrenin et al., 2007; Le Floch et al., 2007). The Goujon model was then forced with surface temperature and accumulation scenarios (see Sect. 3.1.2.) to estimate Δage, allowing producing the ice age scale. It is beyond the scope of this paper to discuss in details this BI preliminary age scale. Sensitivity tests have shown that the underlying dating uncertainties do not affect the results discussed in the following.

No continuous ice and gas chronologies have yet been established for the JRI ice core back to the last glacial period. Our new data are therefore displayed on a depth scale (Fig. 3). The last glacial period is compressed in the last five meters of this ice core. The water stable isotope variation during the last glacial-interglacial transition suggests an unrealistically fast deglaciation compared to all other Antarctic records, related to an unconformity present in the early deglacial interval in the JRI ice core (Mulvaney et al., 2012). These features strongly limit the temporal resolution of measurements that can be conducted on the transition. Using measurements of $\delta^{18}O_{atm}$, a global gas marker (e.g. Bender et al., 1994; Capron et al., 2010), we unequivocally identified samples corresponding to the Early Holocene (EH) and the glacial period (Fig. 3; see Appendix 1 for a full description of Fig. 3 and more details about the definition of chronological constraints).

CPD
8, 6051–6091, 2012

3.3 Temperature and accumulation scenarios as input parameters

When available, surface climatic condition scenarios calculated for establishing the official gas chronologies (Loulergue et al., 2007; Buiron et al., 2011) have been used as inputs for firn modelling. They are deduced following the procedure described by Parrenin et al. (2007). The past surface temperature and accumulation rates are both estimated from the water isotopic records for each ice core. Detailed equations are given in Table 2.

$$T(z) = T_0 + \alpha_D \Delta\delta D(z) \quad (2)$$

or

$$T(z) = T_0 + \alpha_O \Delta\delta^{18}O(z) \quad (3)$$

$$A(z) = A_0 \exp(\beta \Delta D(z)) \quad (4)$$

A_0 (cm ice eq. yr^{-1}) and T_0 (K) are respectively the surface accumulation rate and temperature for the present are taken for each site as given in Fig. 1. $\Delta\delta D$ ($\Delta\delta^{18}O$) corresponds to the difference between δD ($\delta^{18}O$) at a given depth and the present-day value, δD_0($\delta^{18}O_0$). Note that water isotopic profiles are corrected for the influence of vapour source changes using the mean ocean $\delta^{18}O$ (Bintanja et al., 2005; Parrenin et al., 2007). α_D and α_O represent the spatial slope of the present-day isotopic thermometer while the parameter β controls the glacial-interglacial amplitude of the accumulation rate change. Alternatively to the use of Eq. (4) at EDML (Loulergue et al., 2007), Buiron et al. (2011) calculated a synthetic δD record from the TALDICE $\delta^{18}O_{ice}$ data through the following equation:

$$\delta D = 8 \times \delta^{18}O_{ice} + 10, \quad (5)$$

assuming no change in deuterium excess.

CPD
8, 6051–6091, 2012

For EDML, EDC and TALDICE ice cores, we use the same values of α and β parameters as previously optimized to construct the official ice and gas chronologies for this ice core (Parrenin et al., 2007; Loulergue et al., 2007; Buiron et al., 2011). Table 2 summarizes the respective values of α and β parameters for these scenarios. All these equations rely on the assumption that the isotope-temperature relationship observed today spatially (and driven by distillation processes) remains valid for past changes (e.g. Jouzel et al., 2003). It implies that surface and condensation temperatures co-vary, and requires limited precipitation intermittency biases or changes in moisture source conditions (for temperature estimates); this assumption has been challenged for warmer than present day conditions, based on one atmospheric model (Sime et al., 2009). The uncertainty associated with glacial temperature estimates has been estimated to be −10 % to +30 % (Jouzel et al., 2003).

Estimates of past accumulation rates through Eq. (4) assume that precipitation is thermodynamically driven by the atmospheric moisture holding capacity, and do not take into account possible changes in dynamical processes (e.g. cyclonic precipitation, changes in storm tracks). For example, at the sites of JRI and BI, scenarios of accumulation have not yet been incorporated in ice flow models, which allow inferring β values in best agreement with all available stratigraphic constraints, so that we have a larger uncertainty on the choice of the values for those parameters. For α, we used the classical spatial slope of 0.01656 (Lorius and Merlivat, 1977). Similarly, an investigation of modern spatial relationships between δD and accumulation in Antarctica leads to β equal to 0.0152 (R^2 = 0.50) for high elevation sites (more than 2500 m; Masson-Delmotte et al., 2008). For low elevation sites, a β of 0.0065 is found, albeit with weaker correlation (R^2 = 0.20). For JRI and BI, we tested two different accumulation scenarii for each site (Scenario A with a β equal to 0.0156 and Scenario B with a β equal to 0.0065; Table 2), which allow exploring a large range of modelled δ^{15}N values that can be assessed with our δ^{15}N datasets.

CPD
8, 6051–6091, 2012

4 Results

4.1 Modelled δ^{15}N variations

For all sites, the modelled glacial δ^{15}N mean level is higher than the modelled Early Holocene (EH) δ^{15}N mean level (Figs. 3–7). Such a greater gravitational fractionation during glacial time illustrates a deeper LID under colder conditions. This means that the temperature increase is the dominant factor controlling the LID evolution simulated by firn densification models.

Still, the decrease of modelled δ^{15}N over the last deglaciation is not monotonic for the EDC, BI, EDML and TALDICE sites. Starting from high glacial levels, both the EDC and the EDML δ^{15}N are simulated to decrease during the Antarctic Cold Reversal (ACR) and during the EH cooling which follows the temperature optimum marking the end of the deglaciation. In contrast, the simulated EDC and EDML δ^{15}N are increasing during warming intervals as depicted by δD (start of the deglaciation, warming after the ACR). The δ^{15}N increases are due to the accumulation rate changes that have a significant impact in driving the simulated firn depth evolution during the transition. We have tested two extreme accumulation scenarios to model BI δ^{15}N evolutions. The δ^{15}N evolutions produced by the model forced by the two scenarios follow the accumulation rate forcing deduced from the δD profile apart for (i) the onset of the deglacial warming (LGM to ACR) where scenario B does not produce any trend in the simulated δ^{15}N and (ii) the EH, when the simulated δ^{15}N increase is opposite to the accumulation rate/δD decrease.

The opposite influences of temperature and accumulation rate on firnification processes are illustrated for the TALDICE case by comparing two simulations: (i) an "Acc-$\delta^{15}N_{mod}$"curve which represents δ^{15}N simulated in response to accumulation changes only, and (ii) a "Temp-$\delta^{15}N_{mod}$" curve simulated when considering only the effect of temperature change (Fig. 5a). While the two factors have clearly opposite effects when considered individually, the total modelled δ^{15}N curve is not simply the average of the two δ^{15}N simulations considering each single factor. This is due to non-linear interactions

CPD
8, 6051–6091, 2012

because the accumulation rate influence is different for different temperature levels, and vice versa.

Figure 8 presents an alternative way to visualize the competing effect of accumulation rate and temperature on modelled δ^{15}N. It represents the evolution of modelled δ^{15}N vs. accumulation rate and temperature for the full range of accumulation rates and temperatures reconstructed over the deglaciation for our different sites. For each site, we also indicate the temporal evolution of the "accumulation rate vs. temperature" relation during the last deglaciation estimated from water isotopic profiles.

For BI, the trajectory of the temporal evolution of "accumulation rate vs. temperature" in scenario B clearly intersects the iso-δ^{15}N levels from the lowest to the highest levels. This explains the large δ^{15}N decrease simulated between glacial to interglacial conditions. By contrast, in the cases of BI (scenario A) or TALDICE, their deglacial "accumulation rate vs. temperature" trajectory occurs almost parallel to an iso-δ^{15}N line. In this case, small variations of accumulation rate or temperature around the mean trajectory can create a spurious behaviour of the modelled δ^{15}N with alternative increases and decreases of modelled δ^{15}N. This explains the more complex modelled δ^{15}N curves for BI (scenario A) and TALDICE presented on Figs. 4 and 5.

4.2 Comparing the modelled δ^{15} N with the new δ^{15}N datasets

Figures 3, 5 and 6 display our new δ^{15}N profiles obtained during the last deglaciation at JRI, TALDICE, and BI together with the δ^{15}N records of Termination I at EDML (Fig. 4; Landais et al., 2006) and EDC (Fig. 7; Dreyfus et al., 2007). For all ice core sites, including JRI, we confirm the overall model-data δ^{15}N mismatch for glacial-interglacial δ^{15}N variations, which was previously reported for central Antarctic ice cores (Dreyfus et al., 2010; Caillon et al., 2001; Kawamura, 2000). The fact that this model-data mismatch is also depicted at JRI is a surprise, because JRI surface climatic conditions ($-14\,^{\circ}$C of annual mean temperature, snow accumulation rate of 62 cm water eq. yr^{-1}) (Abram et al., 2011) are warmer than for Greenland deep ice core sites, where firn models perform well for glacial-interglacial variations.

CPD
8, 6051–6091, 2012

At EDC, despite the model data mismatch during glacial time, model and data trends appear coherent for the δ^{15}N increase over the two warming phases of LGM – ACR and ACR – EH, with stronger rate of increase in measurements, e.g. from the ACR to the EH, δ^{15}N data present a ∼ 0.060 ‰ increase while the model simulates a ∼ 0.040 ‰ increase. Similarly, at EDML, the period from the onset of the deglacial warming to the ACR is characterized by a steady 0.060 ‰ increase in measured δ^{15}N, smaller than the modelled ∼ 0.020 ‰ δ^{15}N increase (Fig. 4). However, outside of this interval, no clear coherent features can be observed between modelled and measured EDML δ^{15}N. During the intervals between 27 ka and 18.7 ka and between 14.9 and 7.8 ka, δ^{15}N variations are not coherent with the water stable isotope profile. For example, during the glacial period δD is very stable (variations within 3 ‰) but δ^{15}N data show large variations (with a standard deviation of 0.017 ‰), corresponding to changes in the DCH thickness of about 3 m within a few centuries.

At TALDICE, the trends depicted in measurements and simulations are coherent over the three different phases of the deglaciation and the EH (Fig. 5). As for EDC and EDML, the rate of increase is stronger in the measurements (∼ 0.080 ‰) than simulated (∼ 0.030 ‰) over the LGM-ACR warming.

The high-resolution measurements performed on the BI ice core reveal the largest millennial-scale variations so far measured in an Antarctic δ^{15}N profile (Fig. 6). These variations represent true variations in the DCH thickness as (i) they are significantly larger than the analytical error (less than 0.015 ‰) and (ii) each rapid increase/decrease is defined by several consecutive measurements. Over the LGM-ACR phase, simulated and measured δ^{15}N trends appear consistent, with first a common increase and then a common decrease. Again, the rate of change is much more pronounced in the measured than in the simulated δ^{15}N profiles. Over the three other phases of the deglaciation, much more variability is depicted in the measurements than simulated.

As for EDML, δ^{15}N variations are recorded in periods of flat δD: first, a δ^{15}N decrease of 0.073 ‰ corresponding to a DCH thinning of ∼ 17 m in ∼ 1 ka occurs at 19 ka

CPD
8, 6051–6091, 2012

while no major δD variations are recorded; second, the fastest δ^{15}N variation occurs at 11.2 ka with a δ^{15}N increase of 0.090 ‰ in 170 yr (equivalent to a $\sim$ 20 m DCH increase).

4.3 Summary

This model-data comparison leads to three main conclusions:

- Simulations systematically predict higher glacial δ^{15}N levels than the measured ones. Firn simulations fail to capture the long-term increase over the deglaciation and the model-data mismatch is strongest for sites characterized by a low accumulation rate.
- During specific phases of the deglaciation, the δ^{15}N trends derived from firn modeling are consistent with the measurements for most Antarctic sites. During the LGM-ACR warming, firn simulations produce a δ^{15}N increase driven by accumulation rate increase for all sites, in good qualitative agreement with our measurements.
- At all ice core sites, larger magnitudes of trends and larger levels of variability are depicted by measurements than simulations. This shows that our simulations do not correctly resolve all the processes controlling δ^{15}N variations.

5 What controls glacial-interglacial changes in firn structure?

In the light of our new measurements and simulations, we now assess the three hypotheses given in the introduction to explain the observed δ^{15}N model-data mismatch at EDC, EDML and BI. Hypotheses A (relationships between firn depth and accumulation or temperature) and B (convective zone) assume that the physics of the firnification model is generally fine while Hypothesis C assumes that the mismatch is due to the effect of snow impurity content on densification which is not implemented in firn models.

CPD
8, 6051–6091, 2012

First, Hypothesis C is tested by analysing the phase relationship between δ^{15}N variations and the changes in ice core dust concentration available from EDML, TALDICE, BI and EDC ice cores (Figs. 4–7). If the main control on density evolution is the impurity content, we could expect to observe large changes in δ^{15}N changes at depths where large changes are recorded in markers of impurity content (such as Ca^{2+} or the insoluble dust concentrations). Secondly, in order to disentangle between Hypotheses A and B for the EDML site, we compare the gas/ice offset, seen as the Δdepth, obtained from δ^{15}N with an empirical estimate of the Δdepth during the Laschamp event (~ 41 ka). This method and results are described in Sect. 5.2. Thirdly, assessing the validity of the physics of the firn model relies on the comparison between measured and modelled δ^{15}N in the absence of any convective zone, as summarized in the previous section. We include this information in our final discussion (Sect. 5.3).

5.1 A dust influence on firnification?

For EDML, TALDICE, BI and EDC, we cannot observe any systematic link between changes in records of ice impurity content and δ^{15}N variations on a depth scale (Figs. 4–7). In fact, closer relationships are depicted between δ^{15}N and δD (linked to temperature and accumulation rates) than between δ^{15}N and the dust concentration. For time periods where large variations of δ^{15}N are measured without any concomitant variability in δD, no significant change in the impurity content is recorded either. Because glacial-interglacial changes in dust concentrations strongly co-vary with Antarctic climate changes (e.g. Lambert et al., 2012), it is not possible to separate any effect of impurity content from the impact of parallel changes in surface temperature and accumulation rates. While our data cannot rule out such effect, they do not support changes in impurities to be the main cause of the δ^{15}N variability when it is unrelated to water stable isotope changes. Moreover, the fact that glacial and interglacial δ^{15}N levels measured on the TALDICE ice core are approximately equal is contradictory with the dust hypothesis, which would lead to a smaller LID during glacial time when

CPD
8, 6051–6091, 2012

dust concentrations in snow are higher. These new observations are not in favour of Hypothesis C as the major explanation for all model-data mismatches. However, the link between impurity content and density kinetics may not be linear. Previous studies have highlighted a major role of dust on the modification of ice microstructure (through the pinning of grain boundaries, Durand et al., 2006). Thus, further investigations are required based on e.g. future high-resolution glacial dust concentration (or Ca^{2+}) and $\delta^{15}N$ records, and from an improved quantitative understanding of the links between dust concentrations, grain growth and metamorphism and densification processes.

5.2 Constraints on the EDML Δ depth during the Lachamp event

The following exercise relies on an empirical estimate of the Δdepth independent from both the firn model and $\delta^{15}N$. Following the approach of Loulergue et al. (2007), Δdepth is deduced from the ^{10}Be records over the Laschamp event (41.2 ± 1.6 ka on GICC05; Svensson et al., 2007) in the ice phase and from the CH_4 records in the gas phase. Using independent matching of the gas (CH_4) and ice (^{10}Be) records of the EDML ice core with the NorthGRIP gas and ice records, Loulergue et al. (2007) estimated two empirical Δdepth of 21.4 ± 4.6 m and 23.1 ± 4.6 m at about 1368–1407 m depth. Most of the estimated uncertainty is due to the complicated identification of tie-points between the EDML CH_4 record and the corresponding NorthGRIP $\delta^{18}O_{ice}$ record (see Table 1 and Fig. 3b of their paper for more details).

In order to reduce the uncertainty of the Loulergue et al. (2007) empirical Δdepth estimates, we use an objective method based on the Match protocol (Lisiecki and Lisiecki, 2002) to give the best matching between EDML and NorthGRIP CH_4 records. Our revised match between EDML and NorthGRIP CH_4 records is displayed on Fig. 9. After identifying the CH_4 change concomitant with the ^{10}Be peak on the GICC05 timescale, the corresponding depth (following the notation of Loulergue et al., 2007), can directly be read on the CH_4 record on the EDML depth scale from the correspondence between NorthGRIP and EDML CH_4 records (Fig. 9). We thus obtain two EDML depths

CPD
8, 6051–6091, 2012

corresponding to the depths of CH_4 changes concomitant with the age of the two ^{10}Be peaks: 1390.4 m (instead of 1389.8 m in Loulergue et al., 2007) and 1408.5 m (instead of 1406.4 m in Loulergue et al., 2007). The two revised empirical Δdepth deduced from our approach are slightly larger than the original estimates by Loulergue et al. (2007): 22.0 ± 2.5 m and 25.2 ± 2.5 m instead of 21.4 ± 4.6 m and 23.1 ± 4.6 m, respectively. The uncertainty is linked to the mean resolution of the EDML CH_4 record (2.5 m) and to the rate of CH_4 change (Fig. 9). We see that the CH_4 record undergoes a clear minimum at 1408.5 m corresponding to the second ^{10}Be peak for which we estimate the Δdepth of 25.2 ± 2.5 m. Therefore, we consider this estimate as the most robust. These estimates are on the upper end of the Δdepth deduced from EDML firn modelling based on two different accumulation rate histories (modelled Δdepth of about 22.9 m for Scenario 1 and 21.2 m for Scenario 4 as defined by Loulergue et al., 2007).

Then we compare those empirical Δdepth estimates with a Δdepth estimate based on $\delta^{15}N$ measurements. For this, we assume that $\delta^{15}N$ is a direct indicator of the LID, hence assuming (1) that no significant convective zone affected the firn in the past, (2) that $\delta^{15}N$ only reflects the gravitational settling and (3) that the difference between the LID and the COD does not significantly affect the gas repartition during bubble close-off. We derive the diffusive column height (DCH) from $\delta^{15}N$ using the barometric equation (Eq. 1) and we convert then the DCH to Δdepth through the following equation:

$$\Delta\text{depth} = \text{DCH} \times t \times 0.7 \quad (6)$$

In this equation, we account for the thinning (t) due to ice flow by multiplying by the appropriate thinning factor in the ice flow model. The coefficient 0.7 represents the ratio of mean firn density to ice density, which is required to translate the unthinned ice thickness to firn equivalent thickness. We adopt a 5 % uncertainty to account for variations with respect to firn density profiles as a function of temperature and accumulation rate and varying ice density (Blunier et al., 2004). We also used two different estimates of the thinning factor: (ii) one from the EDML glaciological model of Huybrechts

CPD
8, 6051–6091, 2012

et al. (2007) and (ii) one from the new AICC2012 chronology (Bazin et al., 2012) and consider a 10 % uncertainty linked to this parameter.

Our new δ^{15}N data translate into a Δdepth of 26.8 ± 3 m for the 1360–1410 m depth interval. This is slightly larger that the empirical Δdepth estimates. The existence of a convective zone would lead to a δ^{15}N-based Δdepth smaller than the modelled or empirically derived Δdepth, which is opposite to our observation.

As a conclusion, our new results suggest the absence of a convective zone at EDML at the time of the Laschamp event, which occurs under climatic conditions which are representative of the last glacial period. Parrenin et al. (2012b) had also ruled out a large glacial convective zone at EDC, using a Δdepth-based approach.

5.3 Synthesis

Our study suggests that Hypothesis A (the physics of the firnification model is globally correct) is at least partly valid. Based on this hypothesis, the remaining mismatch between modelled and measured δ^{15}N may be attributed to the following causes:

1. The process of firn deepening in response to deglacial accumulation rate increase is underestimated in the firnification model. The densification might be a more time-controlled phenomenon that a pressure-controlled phenomenon. Indeed, if the densification was only time-controlled, Δage would be constant through time and the LID would be proportional to accumulation.

2. The deglacial increase in Antarctic accumulation rates is underestimated, especially at the end of the deglaciation (from the ACR to the EH) when the disagreement is the largest between modelled and measured δ^{15}N. We give arguments supporting this view below.

The simple relationships used to derive surface climatic conditions from water isotopes were originally developed for the East Antarctic Plateau, where the atmospheric moisture content is controlled by local temperature. However, Masson-Delmotte et al. (2008)

CPD
8, 6051–6091, 2012

depict that the modern relationship between accumulation and isotope (β parameter) remains quite uncertain leading to large uncertainties in the accumulation rate scenarios reconstructed for semi-coastal and coastal areas. Several other studies have already suggested that the water isotope-based approach to infer past accumulation rate might not be well suited for these regions potentially affected by changes in cyclonic activity, changes in precipitation intermittency, moisture source conditions and distillation paths at synoptic and seasonal scales (van Ommen et al., 2004; Monnin et al., 2004; Landais et al., 2006). The value of β may have been varying through time, especially for a site such as BI that encountered very particular site-specific climatic and glaciological changes (R. Mulvaney, personal communication, 2012). Indeed, past changes of local ice sheet topography could have significant impacts on (i) atmospheric circulation and elevation-accumulation-temperature-water stable isotope relationships, and (ii) ice flow, layer thinning and inferred accumulation rates.

At EDML, comparing the continuous thermodynamically-derived accumulation rate with discrete accumulation rates derived from the unstrained layer thickness between volcanic match points (Severi et al., 2007) shows their consistency typically within ±20 %. However, the accumulation rate scenario inferred from volcanic signature matching with the EDC ice core produces accumulation variations during the glacial period that are not linked to any variations in the water isotopic profiles. Further exploring the processes that could induce deviations from simple relationships between accumulation, temperature and precipitation isotopic composition, in relationships with changes in moisture origin, trajectories, and precipitation-temperature covariance at synoptic and seasonal scales needs to be further explored, using transient glacial-interglacial simulations conducted with climate models including water stable isotopes under varying topographies and boundary conditions (e.g. Sime et al., 2012).

Altogether, our results suggest that a large part of the variability in the firn LID is climatically driven through a complex combination of surface temperature and accumulation rate effects during large climatic changes such as over the deglaciation (from the ACR to the EH and from the ACR to the LGM). Our results from BI and EDML

CPD
8, 6051–6091, 2012

strongly suggest that, during relatively stable climatic periods (whether it is a glacial or an interglacial period), factors independent of water stable isotopes may take the control of the firn structure. While glaciological processes specific to BI may be at play, our data could be interpreted to suggest that significant accumulation changes may have occurred that are decorrelated from water isotopic profiles. This emphasises the need for quantitative information on past accumulation rates independently of water stable isotope profiles, perhaps obtainable using high-resolution chemical tracer profiles.

6 Conclusions and perspectives

In this paper, we have presented new measurements and simulations of air δ^{15}N profiles from several Antarctic ice cores spanning the last deglaciation. From our model-data synthesis, we conclude that firn models cannot reproduce the observed glacial δ^{15}N levels. However, for most sites, these models are able to capture the successive patterns of δ^{15}N trends during the deglaciation. Still, the measured δ^{15}N profiles generally display much larger variability than simulated. We have highlighted different δ^{15}N behaviors observed at the different sites. In particular, TALDICE glacial δ^{15}N values are similar to interglacial δ^{15}N values, which disfavours the impurity content impact hypothesis. At BI, we measure strong millennial-scale δ^{15}N variations during climatic intervals associated with relatively flat δD, revealing that processes independent from the water isotopes affect the firn structure at this site. Moreover our new results enable us to rule out the hypothesis of large glacial convective zones as the single explanation for the model-data mismatch. Still, direct constraints on the extent of past convective zone (e.g. based on noble gas isotopic measurements, Severinghaus et al., 2006) are necessary in order to strengthen confidence in our conclusions.

Through our δ^{15}N model and data synthesis, we show that a complex competition between the opposite impacts of changes in surface temperature and accumulation rate is at play during the last deglaciation in Antarctic firns. We suggest that the role of temperature in firnification process may have been overestimated in past studies,

CPD
8, 6051–6091, 2012

while the role of accumulation rate should be revised. These new results highlight the importance of using accurate past surface temperature and accumulation rate to force firnification models. Constraints on past changes of the accumulation rate should be developed independently from water isotopic profiles, especially for coastal sites such as Berkner Island.

New ice cores drilled in West Antarctica (Fletcher Promontory, WAIS) should provide new information on the current and past firn structure in coastal and semi-coastal regions.

Appendix A

Chronological constraints for the JRI ice core based on the $\delta^{18}O_{atm}$ variations

Because of its residence time of 1200 yr compared to the interhemispheric mixing time of 1 yr, past $\delta^{18}O_{atm}$ variations should be synchronously recorded in air trapped in Greenland and Antarctic ice cores. Records of $\delta^{18}O_{atm}$ have been used as a tool to synchronise ice cores (Bender et al., 1994; Blunier et al., 1998; Landais et al., 2003; Capron et al., 2010). Thus, we can infer chronological constraints for the JRI ice core thanks to our new isotopic measurements performed on the air trapped in ice. Indeed, $\delta^{18}O$ of O_2 is measured simultaneously to the $\delta^{15}N$ and $\delta^{18}O_{atm}$ is obtained by correcting the raw data for gravitational isotopic fractionation as followed:

$$\delta^{18}O_{atm} = \delta^{18}O - 2 \times \delta^{15}N \quad \text{(A1)}$$

$\delta^{18}O_{atm}$ is known to vary on orbital timescales in response to the growth of ice sheets and changes in biogeochemical fractionation (Bender et al., 1994; Landais et al., 2010; Severinghaus et al., 2009), with a glacial-interglacial range of about 1.5 ‰. By definition present-day air is associated with nil values for the $\delta^{18}O_{atm}$. Early Holocene values reach −0.3 ‰ and Last Glacial Maximum values are up to 1.2 ‰. Based on those observations, we identify 2 samples corresponding to late glacial air that are associated

CPD
8, 6051–6091, 2012

with $\delta^{18}O_{atm}$ values of 1.0‰ and 0.975‰ and $\delta^{15}N$ equal to 0.133‰ and 0.132‰ respectively. At about 10.4 ka, δ^{18}Oatm value is 0.153‰ and $\delta^{15}N$ is 0.242‰. These chronological constraints allow to infer that the glacial-interglacial change amplitude in $\delta^{15}N$ is of +0.110‰ at JRI.

Acknowledgements. We would like to thank Gabrielle Dreyfus and Jean-Robert Petit for useful comments. We are very grateful to Ailsa Benton, Adrian Bouygues, Emily Ludlow, Gregory Teste and Jack Triest for their help in the logistic involved in the cutting and the transport of the ice samples between LSCE, LGGE and BAS. This work was supported by the CNRS/INSU LEFE Berkner Project. This work was supported by the Natural Environment Research Council through the PSPE program. This work is LSCE contribution number XX.

The publication of this article is financed by CNRS-INSU.

References

Abram, N. J., Mulvaney, R., and Arrowsmith, C.: Environmental signals in a highly resolved ice core from James Ross Island, Antarctica, J. Geophys. Res., 116, D20116, doi:10.1029/2011JD016147, 2011.

Albani, S., Delmonte, B., Maggi, V., Baroni, C., Petit, J.-R., Stenni, B., Mazzola, C., and Frezzotti, M.: Interpreting last glacial to Holocene dust changes at Talos Dome (East Antarctica): implications for atmospheric variations from regional to hemispheric scales, Clim. Past, 8, 741–750, doi:10.5194/cp-8-741-2012, 2012.

Arnaud, L., Barnola, J.-M., and Duval, P.: Physical modeling of the densification of snow/firn and ice in the upper part of polar ice sheets, in: Physics of Ice Core Records, edited by: Hondoh, T., Sapporo, 285–305, 2000.

CPD
8, 6051–6091, 2012

Bender, M., Sowers, T., Dickson, M. L., Orchardo, J., Grootes, P., Mayewski, P. A., and Meese, D. A.: Climate Correlations between Greenland and Antarctica during the Past 100,000 Years, Nature, 372, 663–666, 1994.

Bender, M., Floch, G., Chappellaz, J., Suwa, M., Barnola, J.-M., Blunier, T., Dreyfus, G., Jouzel, J., and Parrenin, F.: Gas age-ice age differences and the chronology of the Vostok ice core, 0–100 ka, J. Geophys. Res., 111, doi:10.1029/2005JD006488, 2006.

Bintanja, R., van de Wal, R. S. W., and Oerlemans, J.: Modelled atmospheric temperatures and global sea levels over the past million years, Nature 437, 125–128, 2005.

Blunier, T., Chappellaz, J., Schwander, J., Dällenbach, A., Stauffer, B., Stocker, T. F., Raynaud, D., Jouzel, J., Clausen, H. B., Hammer, C. U., and Johnsen, S. J.: Asynchrony of Antarctic and Greenland climate change during the last glacial period, Nature, 394, 739–743, 1998.

Blunier, T., Schwander, J., Chappellaz, J., Parrenin, F., and Barnola, J. M.: What was the surface temperature in central Antarctica during the last glacial maximum?, Earth Planet. Sc. Lett., 218, 379–388, 2004.

Buiron, D., Chappellaz, J., Stenni, B., Frezzotti, M., Baumgartner, M., Capron, E., Landais, A., Lemieux-Dudon, B., Masson-Delmotte, V., Montagnat, M., Parrenin, F., and Schilt, A.: ALDICE-1 age scale of the Talos Dome deep ice core, East Antarctica, 7, 1–16, 2011.

Caillon, N., Severinghaus, J. P., Jouzel, J., Barnola, J.-M., Kang, J., and Lipenkov, V. Y.: Timing of atmospheric CO_2 and Antarctic temperature changes across termination III, Science, 299, 1728–1731, 2001.

Capron, E., Landais, A., Lemieux-Dudon, B., Schilt A., Masson-Delmotte, V., Buiron, D., Chappellaz, J., Dahl-Jensen, D., Johnsen, S. J., Leuenberger, M., Loulergue, L., and Oerter, H.: Synchronising EDML and NorthGRIP ice cores using $\delta^{18}O$ of atmospheric oxygen ($\delta^{18}O_{atm}$) and CH_4 measurements over MIS 5 (80–123 kyr), Quaternary Sci. Rev., 29, 222–234, 2010.

Courville, Z. R., Albert, M. R., Fahnestock, M. A., Cathles, L. M., and Shuman, C. M.: Impacts of an accumulation hiatus on the physical properties of firn at a low-accumulation polar site, J. Geophys. Res., 490, F02030, doi:10.1029/2005JF000429, 2007.

Durand, G., Weiss, J., Lipenkov, V., Barnola, J.-M., Krinner, G., Parrenin, F., Delmonte, B., Ritz, C., Duval, P., Rothlisberger, R., and Bigler, M.: Effect of impurities on grain growth in cold ice sheets, J. Geophys. Res., 111, F01015, doi:10.1029/2005JF000320, 2006.

EPICA community members: Eight glacial cycles from an Antarctic ice core, Nature, 429, 623–628, 2004.

CPD
8, 6051–6091, 2012

EPICA community members: One-to-one coupling of glacial climate variability in Greenland and Antarctica, Nature, 444, 195–198, 2006.
Fischer, H., Wahlen, M., Smith, J., Mastroianni, D., and Deck, B. L.: Ice core records of atmospheric CO_2 around the last three glacial terminations, Science, 283, 1712–1714, 1999.
Fischer, H., Fundel, F., Ruth, U., Twarloh, B., Wegner, A., Udisti, R., Becagli, S., Castellano, E., Morganti, A., Severi, M., Wolff, E., Littot, G., Röthlisberger, R., Mulvaney, R., Hutterli, M., Kaufmann, P., Federer, U., Lambert, F., Bigler, M., Hansson, M. E., Jonsell, U., de Angelis, M., Boutron, C. F., Siggaard-Andersen, M.-L., Steffensen, J.-P., Barbante, C., Gaspari, V., Gabrielli, P., and Wagenbach, D.: Reconstruction of millennial changes in dust emission, transport and regional sea ice coverage using the deep EPICA ice cores from the Atlantic and Indian Ocean sector of Antarctica, Earth Planet. Sc. Lett., 260, 340–354, 2007.
Goujon, C., Barnola, J.-M., and Ritz, C.: Modeling the densification of polar firn including heat diffusion: Application to close-off characteristics and gas isotopic fractionation for Antarctica and Greenland sites, J. Geophys. Res., 108, 4792, doi:10.1029/2002JD003319, 2003.
Herron, M. and Langway, C.: Firn densification: an empirical model, J. Glaciol., 25, 373–385, 1980.
Huber, C., Leuenberger, M., Spahni, R., Flückiger, J., Schwander, J., Stocker, T. F., Johnsen, S., Landais, A., and Jouzel, J.: Isotope calibrated Greenland temperature record over Marine Isotope Stage 3 and its relation to CH_4, Earth Planet. Sc. Lett., 243, 504–519, 2006.
Huybrechts, P., Rybak, O., Pattyn, F., Ruth, U., and Steinhage, D.: Ice thinning, upstream advection, and non-climatic biases for the upper 89 % of the EDML ice core from a nested model of the Antarctic ice sheet, Clim. Past, 3, 577–589, doi:10.5194/cp-3-577-2007, 2007.
Johnsen, S. J., Dahl-Jensen, D., Gundestrup, N., Steffensen, J. P., Henrick, B., Clausen, H. B., Miller, H., Masson-Delmotte, V., Sveinbjornsdottir, A., and White, J. W. C.: Oxygen isotope and palaeotemperature records from six Greenland ice-core stations: Camp Century, Dye-3, GRIP, GISP2, Renland and NorthGRIP, J. Quat. Sci., 16, 299–307, 2001.
Jouzel, J., Vimeux, F., Caillon, N., Delaygue, G., Hoffmann, G., Masson-Delmotte, V., and Parrenin, F.: Magnitude of the isotope/temperature scaling for interpretation of central Antarctic ice cores, J. Geophys. Res., 108, 1029–1046, 2003.
Jouzel, J., Masson-Delmotte, V., Cattani, O., Dreyfus, G., Falourd, S., Hoffmann, G., Minster, B., Nouet, J., Barnola, J.-M., Fisher, H., Gallet, J.-C., Johnsen, S., Leuenberger, M., Loulergue, L., Luethi, D., Oerter, H., Parrenin, F., Raisbeck, G., Raynaud, D., Schilt, A., Schwander, J., Selmo, J., Souchez, R., Spahni, R., Stauffer, B., Steffensen, J. P., Stenni, B., Stocker, T. F.,

CPD
8, 6051–6091, 2012

Tison, J.-L., Werner, M., and Wolff, E. W.: Orbital and millennial Antarctic climate variability over the past 800,000 years, Science, 317, 793–796, 2007.
Kawamura, K.: Variations of atmospheric components over the past 340 000 years from Dome Fuji ice core, Antarctica, Tohoku, 2000.
Kawamura, K., Severinghaus, J. P., Ishidoya, S., Sugawara, S., Hashida, G., Motoyama, H., Fujii, Y., Aoki, S., and Nakazawa, T.: Convective mixing of air in firn at four polar sites, Earth Planet. Sc. Lett., 244, 672–682, 2006.
Lambert, F., Bigler, M., Steffensen, J. P., Hutterli, M., and Fischer, H.: Centennial mineral dust variability in high-resolution ice core data from Dome C, Antarctica, Clim. Past, 8, 609–623, doi:10.5194/cp-8-609-2012, 2012.
Landais, A., Caillon, N., Severinghaus, J., Jouzel, J., and Masson-Delmotte, V.: Analyses isotopiques à haute précision de l'air piégé dans les glaces polaires pour la quantification des variations rapides de température: méthodes et limites, Notes des activités instrumentales de l'IPSL note no. 39, 2003.
Landais, A., Barnola, J. M., Masson-Delmotte, V., Jouzel, J., Chappellaz, J., Caillon, N., Huber, C., Leuenberger, M., and Johnsen, S. J.: A continuous record of temperature evolution over a sequence of Dansgaard-Oeschger events during Marine Isotopic Stage 4 (76 to 62 kyr BP), Geophys. Res. Lett., 31, L22211, doi:10.1029/2004GL021193, 2004.
Landais, A., Barnola, J.-M., Kawamura, K., Caillon, N., Delmotte, M., Van Ommen, T., Dreyfus, G., Jouzel, J., Masson-Delmotte, V., Minster, B., Freitag, J., Leuenberger, M., Schwander, J., Huber, C., Etheridge, D., and Morgan, V.: Firn-air δ^{15}N in modern polar sites and glacial-interglacial ice: a model-data mismatch during glacial periods in Antarctica?, Quaternary Sci. Rev., 25, 49–62, 2006.
Landais, A., Dreyfus, D., Capron, E., Sanchez-Goni, M. F., Desprat, S., Jouzel, J., Hoffmann, G., and Johnsen, S.: What drives orbital- and millennial-scale variations of the δ^{18}O of atmospheric oxygen?, Quaternary Sci. Rev., 29, 235–246, 2010.
Le Floch, M., Loulergue, L., Barnola, J. M., Raynaud, D., Chappellaz, J., Spahni, R., and Mulvaney, R.: CO_2 and CH_4 measurements on the Berkner ice core: a constrain for evaluating the continuity and the chronology of the record, Geophys. Res. Abstr., EGU2007-06665, EGU General Assembly 2007, Vienna, Austria, 2007.
Lisiecki, L. E. and Lisiecki, P. A.: Application of dynamic programming to the correlation of paleoclimatic records, Paleoceanography, 17, 1049, doi:10.1029/2001PA000733, 2002.

CPD
8, 6051–6091, 2012

Lorius, C. and Merlivat, L.: Distribution of mean surface stable isotope values in East Antarctica. Observed changes with depth in a coastal area, in: Isotopes and impurities in snow and ice, edited by IAHS Publication, Vienna, IAHS-P., 125–137, 1977.

Loulergue, L., Parrenin, F., Blunier, T., Barnola, J.-M., Spahni, R., Schilt, A., Raisbeck, G., and Chappellaz, J.: New constraints on the gas age-ice age difference along the EPICA ice cores, 0–50 kyr, Clim. Past, 3, 527–540, doi:10.5194/cp-3-527-2007, 2007.

Loulergue, L., Schilt, A., Spahni, R., Masson-Delmotte, V., Blunier, T., Lemieux, B., Barnola, J.-M., Raynaud, D., Stocker, T. F., and Chappellaz, J.: Orbital and millennial-scale features of atmospheric CH_4 over the past 800,000 years, Nature, 453, 383–386, 2008.

Lüthi, D., Le Floch, M., Bereiter, B., Blunier, T., Barnola, J.-M., Siegenthaler, U., Raynaud, D., Jouzel, J., Fischer, H., Kawamura, K., and Stocker, T. F.: High-resolution carbon dioxide concentration record 650,000–800,000 years before present, Nature, 453, 379–382, 2008.

Monnin, E., Indermühle, A., Dällenbach, A., Flückiger, J., Stauffer, B., Stocker, T. F., Raynaud, D., and Barnola, J.-M.: Atmospheric CO_2 concentrations over the last glacial terminaison, Science, 291, 112–114, 2001.

Mulvaney, R., Abram, N. J., Hindmarsh, R. C. A., Arrowsmith, C., Fleet, L., Triest, J., Sime, L. C., Alemany, O., and Foord, S.: Recent Antarctic Peninsula warming relative to Holocene climate and ice-shelf history, Nature, 489, 141–144, doi:10.1038/nature11391, 2012.

NorthGRIP community members: High-resolution record of Northern Hemisphere climate extending into the last interglacial period, Nature, 431, 147–151, 2004.

Parrenin, F., Rémy, F., Ritz, C., Siegert, M., and Jouzel, J.: New modeling of the Vostok ice flow line and implication for the glaciological chronology of the Vostok ice core, Antarctica, J. Geophys. Res., 109, D20102, doi:10.1029/2004JD004561, 2004.

Parrenin, F., Barnola, J.-M., Beer, J., Blunier, T., Castellano, E., Chappellaz, J., Dreyfus, G., Fischer, H., Fujita, S., Jouzel, J., Kawamura, K., Lemieux-Dudon, B., Loulergue, L., Masson-Delmotte, V., Narcisi, B., Petit, J.-R., Raisbeck, G., Raynaud, D., Ruth, U., Schwander, J., Severi, M., Spahni, R., Steffensen, J. P., Svensson, A., Udisti, R., Waelbroeck, C., and Wolff, E.: The EDC3 chronology for the EPICA Dome C ice core, Clim. Past, 3, 485–497, doi:10.5194/cp-3-485-2007, 2007.

Parrenin, F., Masson-Delmotte, V., Kölher, P., Raynaud, D., Paillard, D., Schwander, J., Barbante, C., Landais, A., Wegner, A., and Jouzel, J.: Synchronous change in atmospheric CO_2 and Antarctic temperature during the last deglacial warming, in review, 2012a.

CPD
8, 6051–6091, 2012

Parrenin, F., Barker, S., Blunier, T., Chappellaz, J., Jouzel, J., Landais, A., Masson-Delmotte, V., Schwander, J., and Veres, D.: On the gas-ice depth difference (δdepth) along the EPICA Dome C ice core, Clim. Past, 8, 1239–1255, doi:10.5194/cp-8-1239-2012, 2012b.

Pedro, J. B., van Ommen, T. D., Rasmussen, S. O., Morgan, V. I., Chappellaz, J., Moy, A. D., Masson-Delmotte, V., and Delmotte, M.: The last deglaciation: timing the bipolar seesaw, Clim. Past, 7, 671–683, doi:10.5194/cp-7-671-2011, 2011.

Pimienta, P.: Etude de comportement mécanique des glaces polycristallines aux faibles contraintes; application aux glaces de calotte polaire, Thèse de doctorat, Université Joseph Fourrier, 1987.

Ruth, U., Barbante, C., Bigler, M., Delmonte, B., Fischer, H., Gabrielli, P., Gaspari, V., Kaufmann, P. R., Lambert, F., Maggi, V., Marino, F., Petit, J.-R., Udisti, R., Wagenbach, D., Wegner, A., and Wolff, E. W.: Proxies and measurement techniques for mineral dust in Antarctic ice cores, Environ. Sci. Technol., 42, 675–5681, doi:10.1021/es703078z, 2008.

Schilt, A., Baumgartner, M., Blunier, T., Schwander, T., Spahni, R., Fischer, H., and Stocker, T. F.: Glacial-interglacial and millennial-scale variations in the atmospheric nitrous oxide concentration during the last 800,000 years, Quaternary Sci. Rev., 29, 182–192, 2010.

Schwander, J., Barnola, J. M., Andrie, C., Leuenberger, M., Ludin, A., Raynaud, D., and Stauffer, B.: Age scale of the air in the summit ice: Implication for glacial-interglacial temperature change, J. Geophys. Res., 98, 2831–2838, 1993.

Severi, M., Becagli, S., Castellano, E., Morganti, A., Traversi, R., Udisti, R., Ruth, U., Fischer, H., Huybrechts, P., Wolff, E., Parrenin, F., Kaufmann, P., Lambert, F., and Steffensen, J. P.: Synchronisation of the EDML and EDC ice cores for the last 52 kyr by volcanic signature matching, Clim. Past, 3, 367–374, doi:10.5194/cp-3-367-2007, 2007.

Severinghaus, J. P., Grachev, A., and Battle, M.: Thermal fractionation of air in polar firn by seasonal temperature gradients, Geochem. Geophy. Geosy., 2, 1048, doi:10.1029/2000GC000146, 2001.

Severinghaus, J. P., Kawamura, K., and Headly, M. A.: Evidence of deep air convection in firn at Vostok, Antarctica in the penultimate glacial maximum from precise measurements of krypton isotopes, EOS T. Am. Geophys. Un., 87, Fall Meet. Suppl., Abstract U33C-03, 2006.

Severinghaus, J. P., Beaudette, R. A., Headly, M., Taylor, K., and Brook, E. J.: Oxygen-18 of O_2 records the impact of abrupt climate change on the terrestrial biosphere, Science, 324, 1431–1434, 2009.

CPD
8, 6051–6091, 2012

Severinghaus, J. P., Albert, M. R., Courville, Z. R., Fahnestock, M. A., Kawamura, K., Montzka, S. A., Mühle, J., Scambos, T. A., Shields, E., Shuman, C. A., Suwa, M., Tans, P., and Weiss, R. F.: Deep air convection in the firn at a zero-accumulation site, central Antarctica, Earth Planet. Sc. Lett., 293, 359–367, doi:10.1016/j.epsl.2010.03.003, 2010.

Shakun, J. D., Clark, P. U., He, F., Marcott, S. A., Mix, A. C., Liu, Z., Otto-Bliesner, B., Schmittner, A., and Bard, E.: Global warming preceded by increasing carbon dioxide concentrations during the last deglaciation, Nature, 484, 49–54, doi:10.1038/nature10915, 2012.

Sime, L. C., Risi, C., Tindall, J. C., Sjolte, J., Wolff, E. W., Masson-Delmotte, V., and Capron, E.: Warm climate isotopic simulations: What do we learn about interglacial signals in Greenland ice cores?, Quaternary Sci. Rev., submitted, 2012.

Sowers, T. A., Bender, M. L., and Raynaud, D.: Elemental and isotopic composition of occluded O_2 and N_2 in polar ice, 94, 5137–5150, 1989.

Sowers, T. A., Bender, M., Raynaud, D., and Korotkevich, Y. S.: δ^{15}N of N_2 in air trapped in polar ice: a tracer of gas transport in the firn and a possible constraint on ice age-gas differences, J. Geophys. Res., 97, 15683–15697, 1992.

Stenni, B., Selmo, E., Masson-Delmotte, V., Oerter, H., Meyer, H., Röthlisberger, R., Jouzel, J., Cattani, O., Falourd, S., Fischer, H., Hoffmann, G., Lacumin, P., Johnsen, S. J., and Minster, B.: The deuterium excess records of EPICA Dome C and Dronning Maud Land ice cores (East Antarctica), Quaternary Sci. Rev., 29, 146–159, 2010.

Stenni, B., Buiron, D., Frezzotti, M., Albani, S., Barbante, C., Bard, E., Barnola, J.-M., Baroni, M., Baumgartner, M., Bonazza, M., Capron, E., Castellano, E., Chappellaz, J., B. Delmonte, B., Falourd, S., Genoni, L., Lacumin, P., Jouzel, J., Kipfstuhl, S., Landais, A., Lemieux-Dudon, B., Maggi, V., Masson-Delmotte, V., Mazzola, C., Minster, B., Montagnat, M., Mulvaney, R., Narcisi, B., Oerter, H., Parrenin, F., Petit, J. R., Ritz, C., Scarchilli, C., Schilt, A., Schüpbach, S., Schwander, J., Selmo, E., Severi, M., Stocker, T. F., and Udisti, R.: Expression of the bipolar seesaw in Antarctic climate records during the last deglaciation, Nat. Geosci., 4, 46–49, 2011.

Svensson, A., Andersen, K. K., Bigler, M., Clausen, H. B., Dahl-Jensen, D., Davies, S. M., Johnsen, S. J., Muscheler, R., Rasmussen, S. O., Rothlisberger, R., Steffensen, J. P., and Vinther, B. M.: The Greenland Ice Core Chronology 2005: 15–42 ka. Part 2: comparison to others records, Quaternary Sci. Rev., 25, 3258–3267, 2007.

CPD
8, 6051–6091, 2012

Table 1. New and published δ^{15}N measurements performed on EDML, JRI, BI and TALDICE ice cores and associated analytical uncertainties.

Ice core	Measurements time period	Number of depth levels with duplicate measurements	Pooled standard deviation (‰)	Time interval (ka)	Mean temporal resolution (yr)
JRI	Spring 2011	20	0.005	At least the last glacial/interglacial cycle	NaN
BI	Spring 2007	51	0.015	3.8–20.6	184
	Spring 2010	59	0.007		
TALDICE	Winter 2010	33	0.008	8.9–23.9 (8.9–18.4)	358 (260)
EDML	Landais et al. (2007)	51	0.006	7.9-41.2	457
	Spring 2007	21	0.022		

CPD
8, 6051–6091, 2012

Table 2. Information about each ice core: description of available chronologies and methods, parameters relating water stable isotopes, temperature and accumulation, and estimated LGM surface conditions (temperature and accumulation rates).

Ice core site (official chronology name)	Chronology available	Method	References	α and β parameters values	LGM T (°C) and A (cm ice eq. per yr)
EDC(EDC3)	Ice	Inverse dating method	Parrenin et al. (2007)	$\alpha_D = 0.1656$ $\beta = 0.0157$	$T = -63$ $A = 1.2–1.4$
	Gas	Firn densification model Goujon et al. (2003)	Loulergue et al. (2007)		
EDML (EDML1)	Ice	Synchronisation to EDC through volcanic markers	Ruth et al. (2007)	$\alpha_O = 1.220$ $\beta = 0.0120$	$T = -54$ $A = 3.3–3.7$
	Gas	Firn densification model Goujon et al. (2003)	Loulergue et al. (2007)		
TALDICE (TALDICE1)	Ice/Gas	Inverse dating method (Lemieux Dudon et al., 2010)	Buiron et al. (2011)	$\alpha_D = 0.1984$ $\beta = 0.0165$	$T = -52$ $A = 3.1–3.5$
BI	Ice	Firn densification modeling	R. Mulvaney, personal communication (2012)	$\alpha_D = 0.1656$ $\beta_A = 0.0150$ $\beta_B = 0.0065$	$T = -44$ $A_1 = 2.0–2.5$ $A_2 = 5.9–6.4$
	Gas	CO_2 and CH_4 record matching	R. Mulvaney, personal communication (2012)		
JRI	Gas	$\delta^{18}O_{atm}$ record	This study	$\alpha_D = 0.1656$ $\beta_A = 0.0150$ $\beta_B = 0.0065$	$T = -20$ $A_1 = 30.1–30.6$ $A_2 = 44.5–45$

CPD
8, 6051–6091, 2012

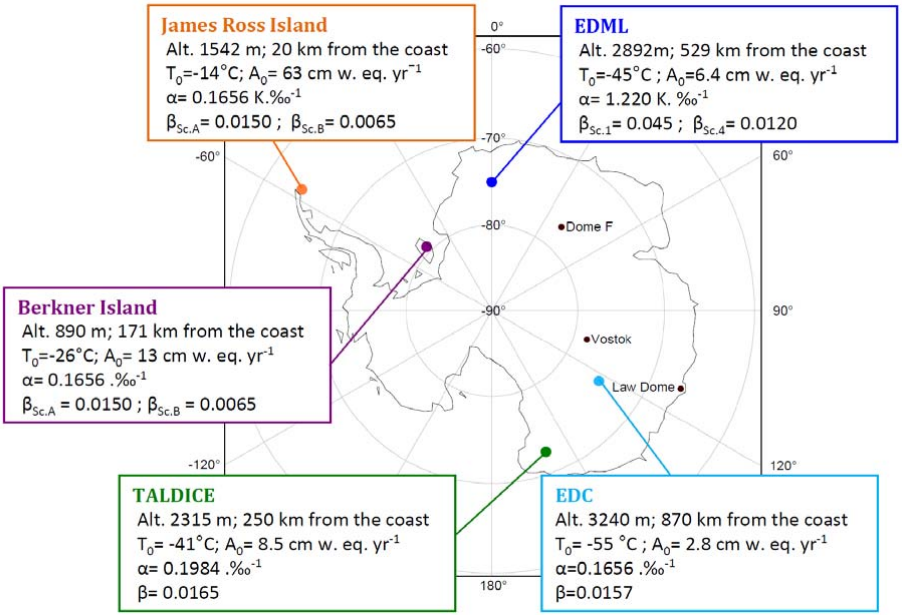

Fig. 1. Location of the Antarctic ice cores where δ^{15}N measurements have been conducted during the last deglaciation. The altitude, the distance from the coast, the mean annual surface temperature, T_0 (in degree Celcius), and the accumulation rate, A_0 (in water equivalent per year) are indicated for the ice core sites discussed in this study (Abram et al., 2011; Buiron et al., 2011; EPICA community members, 2004, 2006; Loulergue et al., 2007; Mulvaney et al., 2000, 2012; Parrenin et al., 2007; Stenni et al., 2011).

CPD
8, 6051–6091, 2012

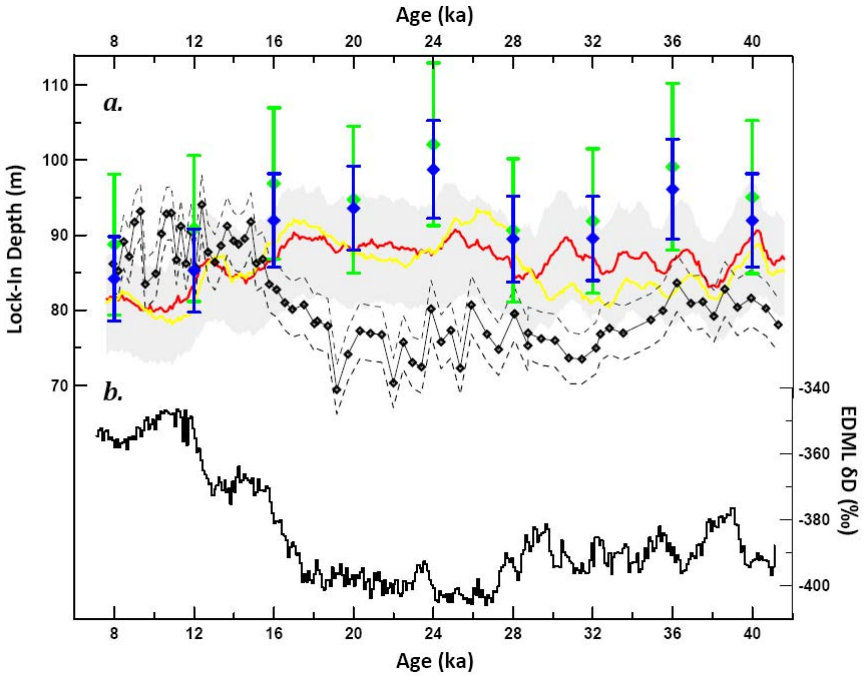

Fig. 2. EDML Lock In-Depth (LID) evolution over the last deglaciation using three firn densification models of different levels of complexity forced by the same climatic history: (i) model of Herron and Langway (1980) (green diamonds); (ii) model of Arnaud et al. (2000)(blue diamonds); (iii) model of Goujon et al. (2003)(red curve). Error bars on simulated LID represent a 30 % uncertainty on the past accumulation rate estimate. Similarly with the grey area for the Goujon simulated curve. An alternative accumulation rate scenario deduced from volcanic stratigraphic markers (Severi et al., 2007) is also used to force the Goujon model (yellow curve). Diffusive Column Height (DHC) deduced from δ^{15}N measurements (opened black diamond curve, Landais et al., 2006) accounting for a 20 % uncertainty on the temperature estimate (black dotted curves).

CPD
8, 6051–6091, 2012

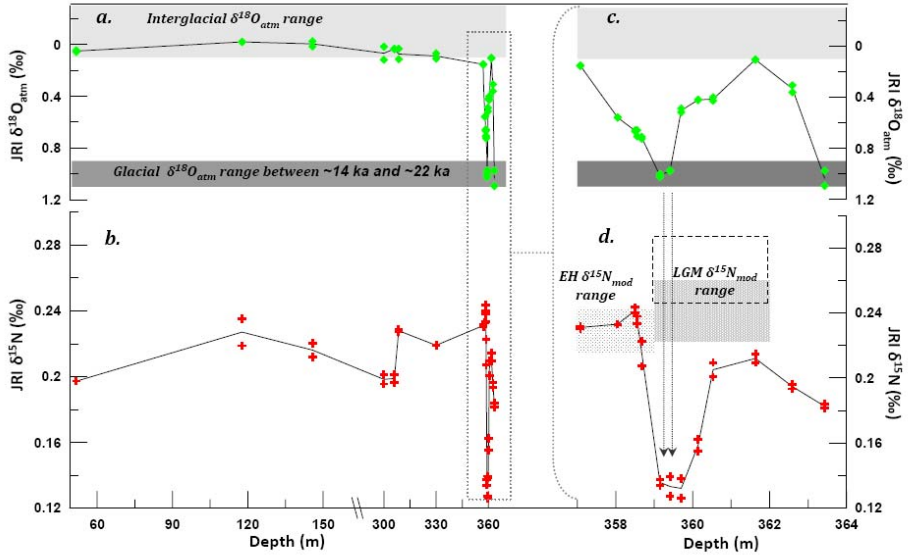

Fig. 3. Air isotopic measurements on the JRI ice core **(a)** $\delta^{18}O_{atm}$ (green diamonds). Black curve fits the average value for each depth level. **(b)** $\delta^{15}N$ (red crosses). Black curve fits the average value for each depth level. **(c)** and **(d)** are a zoom on the depth interval 357–364 m. On panels **(a)** and **(c)**, the light grey area represents the typical $\delta^{18}O_{atm}$ values measured during interglacial (between −0.3 and 0.1 ‰; e.g. Severinghaus et al., 2008). The dark grey area represents the typical $\delta^{18}O_{atm}$ values measured during the glacial period (between 1.1 and 0.9 ‰). The dotted arrows indicate two $\delta^{15}N$ data points that have been unambiguously measured on air from glacial ice. The dotted light grey area represents the modelled $\delta^{15}N$ range for EH and the dotted dark grey area represents the modelled $\delta^{15}N$ range for the LGM based on the Arnaud model.

CPD
8, 6051–6091, 2012

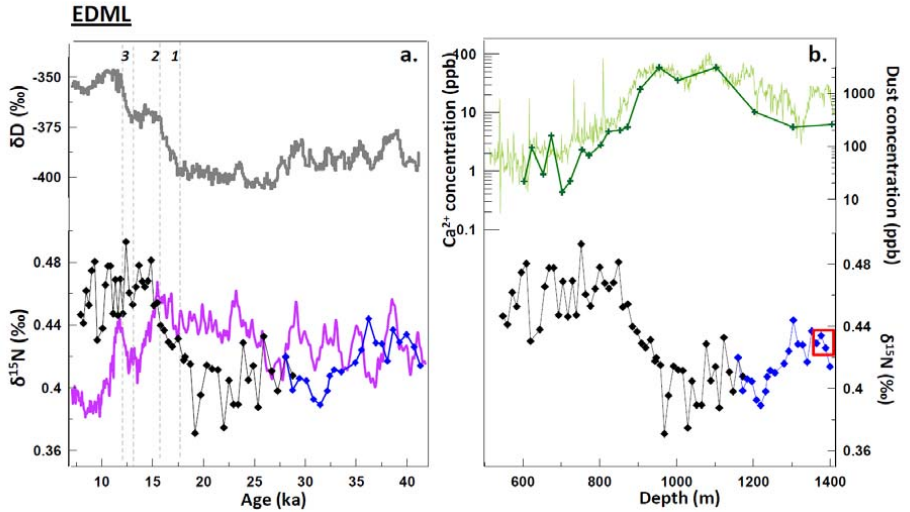

Fig. 4. Experimental and model results for EDML. Three phases over the deglaciation (1 – from the LGM to the ACR; 2 – the ACR; 3 – from the end of the ACR to the EH) are indicated by vertical dashed light grey lines. **(a)** From top to bottom on the Loulergue et al. (2007) age scale: δD profile (grey, Stenni et al., 2010), published δ^{15}N data (black diamonds, Landais et al., 2006), new δ^{15}N data (blue diamonds) and modelled δ^{15}N (purple curve). **(b)** From top to bottom on a depth scale: dust concentration profile (light green; Ruth et al., 2008) and Ca^{2+} concentration (dark green; Fischer et al., 2007), δ^{15}N data (black diamonds; Landais et al., 2006) and new δ^{15}N data (blue diamonds). Red rectangle highlights δ^{15}N data used to infer Δdepth estimates (from 1363.2 m to 1387.8 m).

CPD
8, 6051–6091, 2012

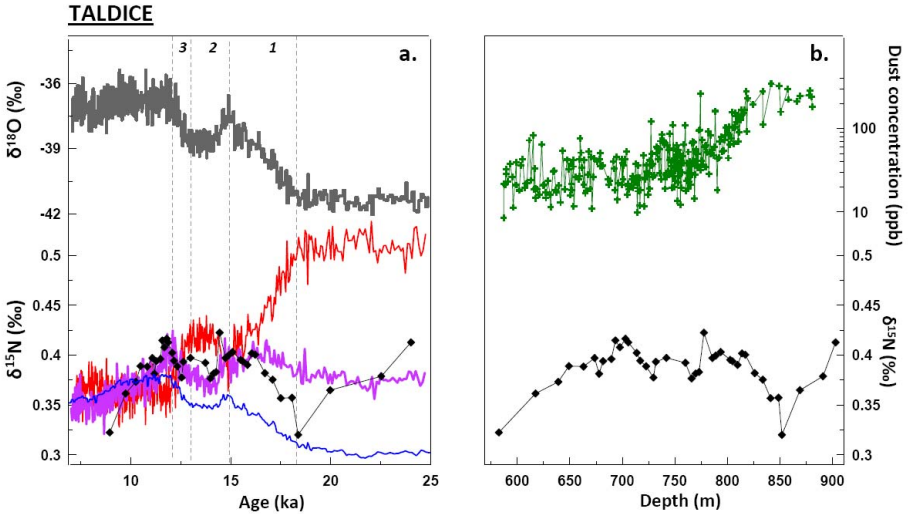

Fig. 5. Experimental and model results for TALDICE. Three phases over the deglaciation (1 – from the LGM to the ACR; 2 – the ACR; 3 – from the end of the ACR to the EH) are indicated by dashed light grey line. **(a)** From top to bottom on the TALDICE1 age scale (Buiron et al., 2011): δD profile (grey; Stenni et al., 2011), new δ^{15}N data (black diamonds), modelled TALDICE δ^{15}N (purple curve), "Acc- $\delta^{15}N_{mod}$" curve (blue) which represents δ^{15}N simulated in response to accumulation changes only, and "Temp-$\delta^{15}N_{mod}$" curve (red) simulated when considering only the effect of temperature change. **(b)** From top to bottom on the depth scale: dust concentration profile (green; Albani et al., 2012) and new δ^{15}N data (black diamonds).

CPD
8, 6051–6091, 2012

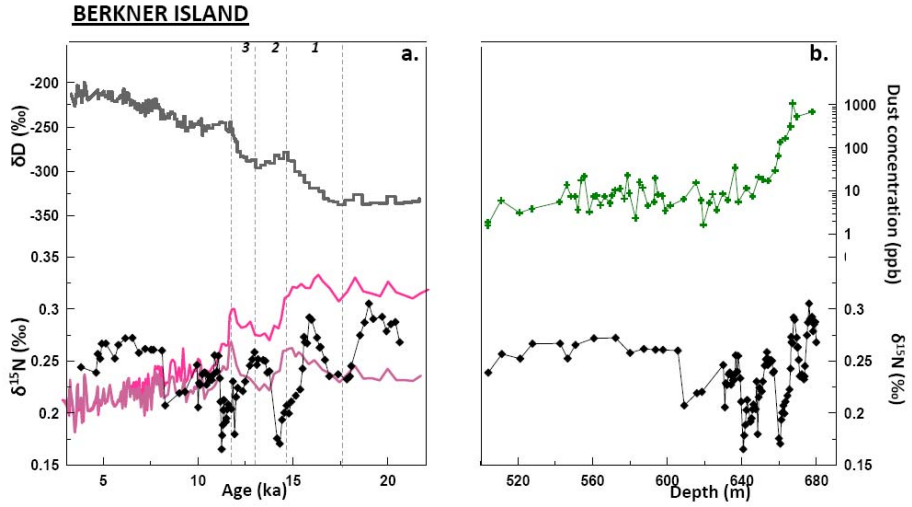

Fig. 6. Experimental and model results for BI. The three phases over the deglaciation (1 – from the LGM to the ACR; 2 – the ACR; 3 – from the end of the ACR to the EH) are separated by dashed light grey line. **(a)** From top to bottom on an age scale (R. Mulvaney, personal communication, 2012): δD profile (grey, R. Mulvaney, personal communication, 2012), new δ^{15}N data (black diamonds), modelled δ^{15}N with Scenario A (β equal to 0.0156; violet curve) and with Scenario B (β equal to 0.0065; pink curve). **(b)** From top to bottom on the depth scale: dust concentration profile (light green; this study, see Lambert et al., 2008, for experimental details for dust concentration measurements) and new δ^{15}N data (black diamonds).

CPD
8, 6051–6091, 2012

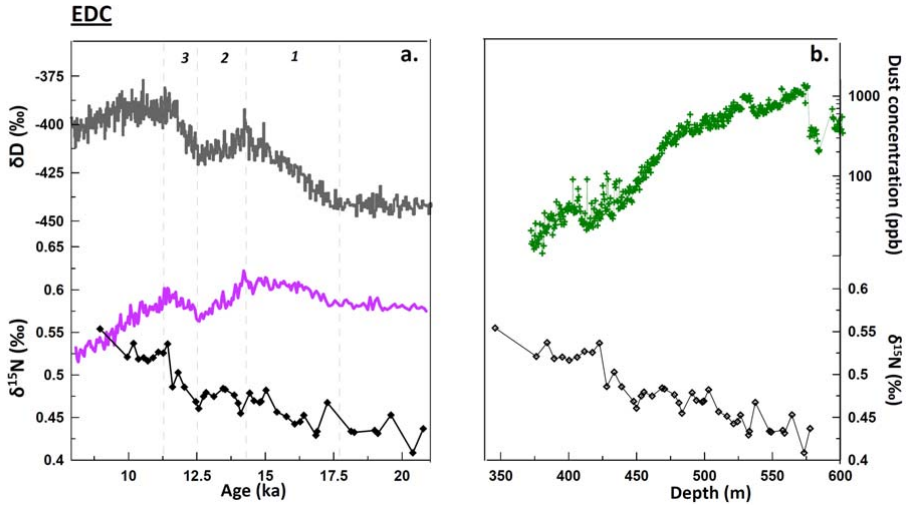

Fig. 7. Experimental and model results for EDC. Three phases over the deglaciation (1 – from the LGM to the ACR; 2 – the ACR; 3 – from the end of the ACR to the EH) are separated by dashed light grey line. **(a)** From top to bottom over Termination I (TI) on the EDC3 age scale: δD profile (grey, Jouzel et al., 2007), δ^{15}N data (Dreyfus et al., 2010) and modelled δ^{15}N (purple curve). **(b)** From top to bottom on the depth scale over Termination I (TI): dust concentration profile (green, Lambert et al., 2012) and δ^{15}N data (Dreyfus et al., 2010).

CPD
8, 6051–6091, 2012

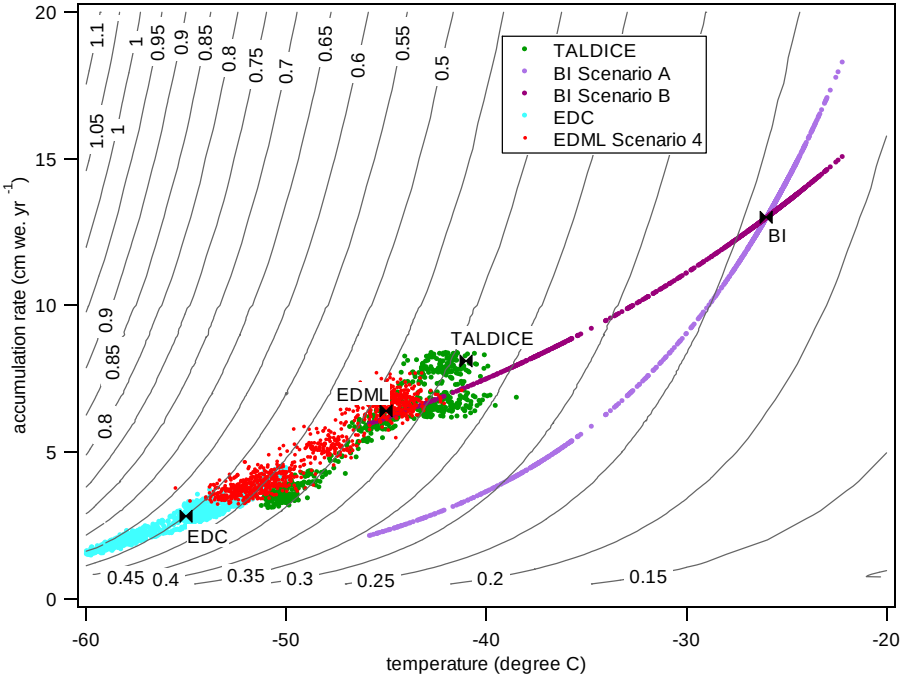

Fig. 8. δ^{15}N evolution (‰) versus accumulation rate and temperature calculated by the Arnaud model (2000). Scenarios of past temperature and accumulation rate evolution are plotted for EDML (red), EDC (turquoise), TALDICE (green) and BI (Scenario A, purple; Scenario B, light purple). Present climatic surface conditions are indicated for each site.

CPD
8, 6051–6091, 2012

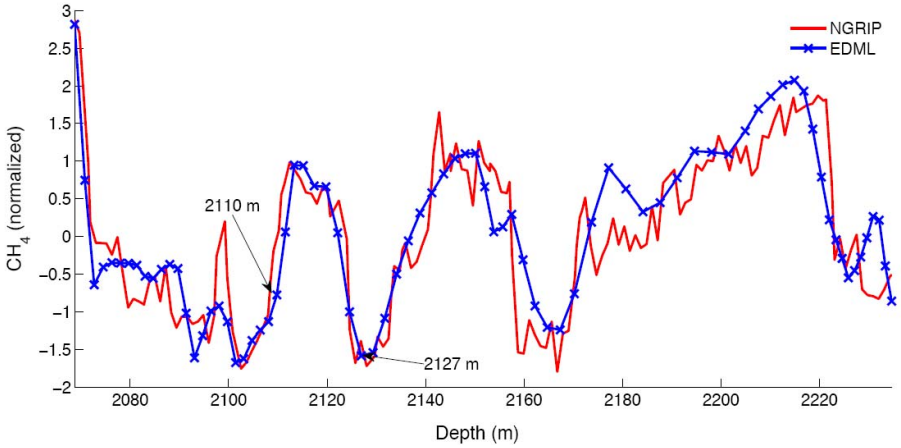

Fig. 9. Synchronization of EDML and NorthGRIP CH_4 records after normalization on the depth scale of NorthGRIP. The two depth levels 2110 and 2127 m correspond to the two ^{10}Be peaks and hence to the EDML depths of 1389.8 and 1408.5 m identified in the gas CH_4 record. We are more confident on the second depth level (noted 2127 m) corresponding to a minimum since it does not depend on the normalization of the records.

CPD
8, 6051–6091, 2012